Editors' Suggestion

Noninvasive LHC transverse beam size measurement using inelastic beam-gas interactions

A. Alexopoulos,[†] C. Barschel, E. Bravin, G. Bregliozzi, N. Chritin, B. Dehning,[§] M. Ferro-Luzzi, M. Giovannozzi, R. Jacobsson, L. Jensen, R. Jones, V. Kain, R. Kieffer,[‡] R. Matev, M. Rihl, V. Salustino Guimaraes, R. Veness, S. Vlachos,[*] and B. Würkner[‖]

CERN, CH-1211 Geneva 23, Switzerland

A. Bay, F. Blanc, S. Giani, O. Girard, G. Haefeli, P. Hopchev, A. Kuonen, T. Nakada, O. Schneider, M. Tobin, and Z. Xu

EPFL Swiss Federal Institute of Technology, CH-1015 Lausanne, Switzerland

R. Greim, T. Kirn, S. Schael, and M. Wlochal

RWTH Aachen University, I. Physikalisches Institut, Sommerfeldstrasse 14 D-52074 Aachen, Germany

(The BGV Collaboration)

(Received 5 February 2019; published 11 April 2019)

The beam-gas vertex (BGV) detector is an innovative instrument measuring noninvasively the transverse beam size in the Large Hadron Collider (LHC) using reconstructed tracks from beam-gas interactions. The BGV detector was installed in 2016 as part of the R&D for the High-Luminosity LHC project. It allows beam size measurements throughout the LHC acceleration cycle with high-intensity physics beams. A precision better than 2% with an integration time of less than 30 s is obtained on the average beam size measured, while the transverse size of individual proton bunches is measured with a resolution of 5% within 5 min. Particles emerging from beam-gas interactions in a specially developed gas volume along the beam direction are recorded by two tracking stations made of scintillating fibers. A scintillator trigger system selects, on-line, events with tracks originating from the interaction region. All the detector elements are located outside the beam vacuum pipe to simplify the design and minimize interference with the accelerated particle beam. The beam size measurement results presented here are based on the correlation between tracks originating from the same beam-gas interaction vertex.

DOI: 10.1103/PhysRevAccelBeams.22.042801

I. INTRODUCTION

The LHC beam-gas vertex (BGV) detector is a noninvasive transverse beam profile monitor developed for the high-luminosity upgrade of the LHC (HL-LHC) [1]. The BGV system reconstructs the transverse beam size by detecting particles from inelastic beam-gas interactions. A gas target chamber is installed in the path of the circulating beam with neon gas injected to create a homogeneous gas volume with which the beam can interact. Particles emerging from the beam-gas interactions are detected by several planes of scintillating fiber detectors (SciFi) to enable high-precision track reconstruction. The transverse beam size is determined using the correlation of the impact parameters (IPs) between the tracks emerging from the same beam-gas interaction. Alternatively, the reconstructed tracks could also be used to estimate the vertex position of each interaction, building up a picture of the transverse beam profile [2,3]. This method was originally developed for the LHCb experiment [4], with, however, the limitation that data could be acquired only during stable beam conditions.

Up to now, noninvasive gas-based beam profile monitors have been based on either gas ionization or fluorescence due to the passage of a particle beam. Residual gas ionization profile monitors (IPMs) reconstruct the beam

[*]Corresponding author.
Also at National Technical University of Athens, Greece.
S.Vlachos@cern.ch
[†]Deceased.
[‡]Also at Royal Holloway College, University of London, United Kingdom.
[§]Also at University of Thessaly, Volos, Greece.
[‖]Also at Technische Universität, Vienna, Austria.

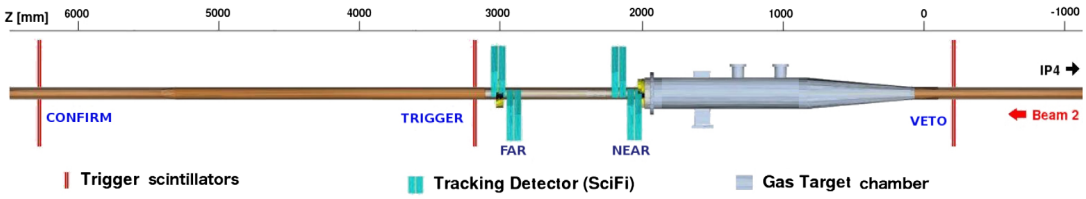

(a) The three main BGV components: The gas target, the tracking detectors and the trigger scintillators.

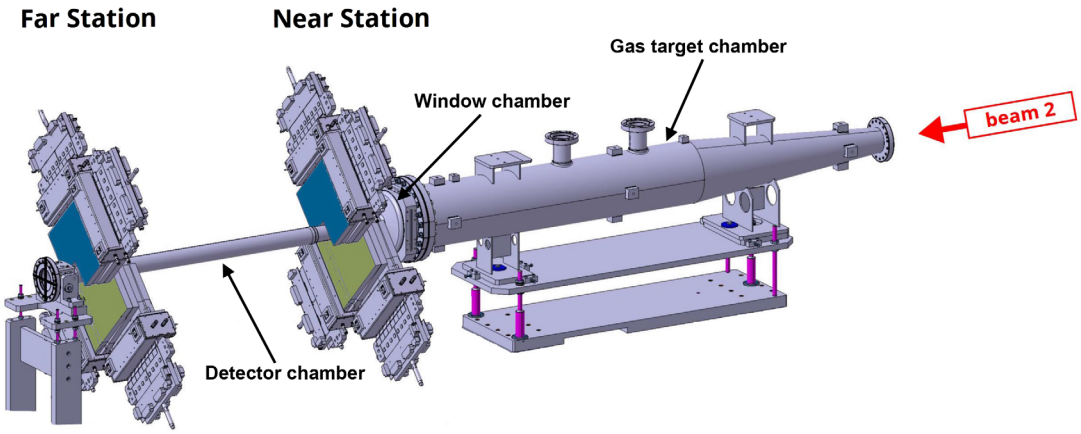

(b) A 3-D view of the SciFi BGV tracker around the LHC beam pipe downstream the Gas target chamber.

FIG. 1. A schematic drawing of the BGV detector.

profile by detecting electrons and/or ions produced from the ionization of the residual gas by the passing accelerated beam particles (see, for example, Ref. [5]). Electric and magnetic fields are used to direct ionization products to the corresponding detectors. On the other hand, beam-induced fluorescence (BIF) monitors detect the image from the fluorescence light emitted after the excitation of the gas by the passing particle beam (see, for example, Ref. [6]). Fluorescence cross sections are relatively small, and, in addition, fluorescence photons are emitted in all directions; the solid angle coverage of a fluorescence detector is of the order of 10^{-4}. Local pressure bumps may be used to increase the signal strength for either IPMs or BIFs [7]. The method presented here is based on detecting the products of beam-gas nuclear inelastic scattering using a transversely uniform gas target. It is, therefore, complementary to the existing ones. It provides fast beam size measurements without introducing any field (electric or magnetic) along the beam path.

The gas pressure in the interaction volume is low enough so as not to perturb the circulating LHC beam but sufficient to allow enough interactions for real-time measurements. In less than 30 s, the transverse beam size can be measured with a precision better than 2%. The gas used and its pressure can be selected to accommodate a large range of beam energies and intensities. Higher pressure and/or longer integration times also allow measurement of the transverse size of individual bunches. Based on the beam size measured, and knowing the β function and dispersion at the location of the BGV, the transverse beam emittance ϵ can be calculated. Furthermore, relative bunch populations and ghost charges (beam population in nominally empty bunch slots) can be quickly estimated using the BGV trigger system, as for these measurements no precise tracking or vertex reconstruction is required.

The BGV demonstrator system is installed at point 4 of the LHC on the counterclockwise (beam 2) ring. It is placed at a point where the β functions in the two transverse dimensions are roughly equal. This allows a circular, reduced-diameter beam pipe to be used, such that the BGV tracker can be as close as possible to the beam line and the interaction region. At the BGV location, for the nominal LHC normalized emittance ($\epsilon_n = 2.5$ μm), the 6.5 TeV proton beam is expected to have a transverse size rms of $\sigma_{x,y} \approx 220$ μm.

The BGV system is composed of three independent objects, described in detail in the next sections: the gas target where beam-gas interactions occur (Sec. II), the trigger system that selects interactions originating from the beam-gas interaction region (Sec. III), and the SciFi precision tracking system (Sec. IV) used to reconstruct tracks and vertices (see Fig. 1). Following these descriptions, the data acquisition and on-line event processing system are presented (Sec. V). The exact analysis method used is described in Sec. VII. Section VIII presents beam size measurements obtained at the end of the 2017 and during the 2018 LHC operation periods. Further developments and conclusions are outlines in Secs. IX and X.

II. GAS TARGET

A dedicated gas target system is used to generate the inelastic beam-gas interactions needed for the BGV operation. It comprises a 3-mm-thin, 1873-mm-long enlarged aperture vacuum chamber containing the gas volume, a gas injection and evacuation system, a very thin exit window, and a 1-m-long reduced aperture vacuum chamber along the LHC beam 2 direction.

The gas target system is designed according to the following requirements: (i) fairly uniform longitudinal gas density over a length of at least 1 m, (ii) uniform transverse gas density over the transverse size of the beam (≈1 mm), (iii) controllable gas pressure (i.e., beam-gas interaction rate), by tuning the gas flow, (iv) no impact on the LHC operation: negligible beam losses and no beam instabilities and no movable parts inside the LHC vacuum, (v) low-mass, large-acceptance exit window for the generated beam-gas interaction particles (thickness corresponding to a radiation length of 1% or less, polar angle range 10–100 mrad), and (vi) thin, reduced-diameter beam pipe diameter in the BGV tracker region, for optimal IP and vertex resolution. A summary of the gas target design and implementation is given in the following sections. Further details can be found in Ref. [8].

A. Design considerations

The target gas in the BGV system needed to fulfil the following criteria: have a large beam-gas interaction rate, be compatible with the nonevaporable getter (NEG) used in the LHC, and avoid saturation of the ion pumps. Neon was therefore selected as the target gas.

The gas target thickness (i.e., target density integrated over the useful length) determines the inelastic beam-gas interaction rate. The rate of inelastic proton-nucleus collisions per bunch can be calculated from

$$R = t_A N f_{\mathrm{rev}} \sigma_{pA}, \tag{1}$$

where t_A is the total target thickness (number of scattering centers per unit area), N is the number of protons per bunch, f_{rev} is the LHC revolution frequency, and σ_{pA} is the inelastic proton-nucleus cross section. The latter can be approximated with $\sigma_{pA} = \sigma_{pp} A^{2/3}$, where σ_{pp} is the inelastic proton-proton cross section [9] (at the equivalent nucleon-nucleon center of mass energy) and A is the mass number of the target gas [10]. The inelastic scattering cross section is substantial for proton energies above 10 GeV. In the energy range from 0.45 to 7 TeV, $\sigma_{p\mathrm{Ne}}$ ranges from about 240 to 300 mb.

The operational pressure in the gas target is typically 1×10^{-7} mbar. This results in a gas target thickness giving an inelastic p-Ne interaction rate of 165 Hz per bunch of 10^{11} protons. In this configuration, the BGV gas target has no impact on the accelerator operation. For comparison, the nominal LHC vacuum is of the order of 1×10^{-10} mbar (mainly hydrogen) [11].

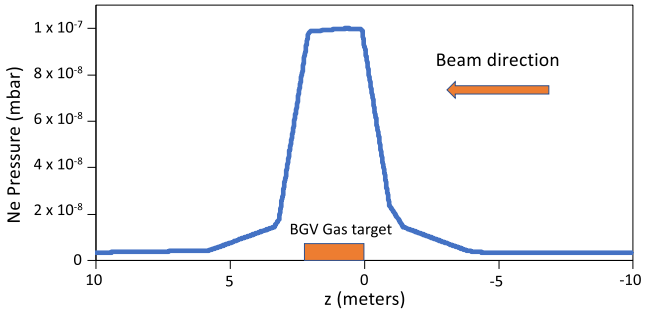

FIG. 2. Simulated longitudinal pressure profile along the BGV vacuum sector.

B. Implementation

Gas is injected into the gas target chamber using a remotely controlled flow valve to maintain the pressure level required (nominally 1×10^{-7} mbar). Ion pumps upstream and downstream evacuate the injected gas. A simulation of the resulting longitudinal pressure profile in the BGV vacuum sector is shown in Fig. 2.

The gas target chamber is 1873 mm long and made out of 3-mm-thick stainless steel (316N). Its effective longitudinal and transverse impedance remain in the background to that of the rest of the accelerator [8]. A 5° taper angle was introduced to minimize wakefield effects on the proton beam.

The exit window of the gas target chamber serves as a low multiple scattering interface for the beam-gas interaction products. This conical exit window reduces in size from an inner diameter of 212 mm to an inner diameter of 52 mm (the minimum allowed by the LHC aperture restrictions [8]). At the same time, the wall thickness decreases linearly from 3.2 (3.6% of a radiation length) to 0.9 mm (1.0% of a radiation length) [12].

The exit window chamber comes with the detector chamber, a 925-mm-long, 58-mm-inner-diameter vacuum tube.

In order to minimize the multiple scattering of emerging particles, both the window and detector chambers are made of the aluminum alloy AA2219. This alloy has a similar yield strength to steel but an approximately 5 times higher radiation length.

Upstream of the gas target chamber, an additional stainless-steel, 53-mm-inner-diameter vacuum tube (the upstream chamber) provides the necessary restriction for efficient gas evacuation. In addition, this reduced diameter gives a better acceptance to the veto scintillators of the trigger system that are placed in this location.

All the BGV vacuum chambers are coated with NEG, which is activated *in situ* [13].

III. THE TRIGGER SYSTEM

A. Scintillator design, placement, and readout

Identification of beam-gas interactions is provided by a dedicated trigger system ($L0$). This trigger system is composed of three scintillator stations (see Fig. 1). Each station consists of two 30 cm × 30 cm 1-cm-thick scintillator plates, placed above and below the beam pipe. The first trigger station (veto) is located upstream of the beam-gas interaction region and is used to reject events with particles originating upstream of the interaction region. The second station (trigger) is placed right after the *far* BGV tracking station with the third station (confirm) placed 3 m further downstream. The time difference between the signals coming from the trigger and confirm stations is used to select particles crossing the BGV detector in the correct direction.

Each scintillator is connected to a 60 mm photomultiplier tube assembly and read out through a constant fraction discriminator. The digital signals are then passed to a programmable logic unit. There they are aligned in time with a precision of better than 1 ns. A decision algorithm provides the output trigger signal. During normal BGV operation, an event is triggered and read out when a coincidence of the trigger and confirm stations is observed in the absence of a signal from the veto station.

B. Trigger performance

Several qualification measurements and a measurement of the relative bunch populations of the LHC beam 2 are performed with the $L0$ trigger system. The time resolution of the trigger detectors is estimated by comparing the arrival time of the signal from the trigger and confirm stations [Fig. 3(a)]. This time difference has an rms of 3 ns, which implies a time resolution per station of approximately 2 ns. Such a good timing performance allows for bunch by bunch beam quality measurements.

Another test of the $L0$ trigger system is performed by measuring the $L0$ trigger rate while varying the pressure inside the gas target chamber. The data collected during a 6.5 TeV LHC fill are shown in Fig. 3(b). The expected linear dependence is observed.

The BGV $L0$ trigger system can be used to perform measurements of the relative bunch populations by exploiting the direct proportionality between the inelastic collision rate and the number of protons per bunch [Eq. (1)]. As an example, Fig. 4 shows the results of one such measurement, performed at a beam energy of 6.5 TeV. To achieve a statistical precision of better than 1% with a gas pressure of 1.3×10^{-7} mbar, the $L0$ trigger rate per bunch is averaged over 61 s. As shown in Fig. 4, the BGV measurement is in good agreement with the relative bunch population estimates obtained with the LHC beam current transformer (BCT), indicating that the BGV $L0$ trigger rate can be used as an independent, stand-alone measurement of the relative bunch intensity.

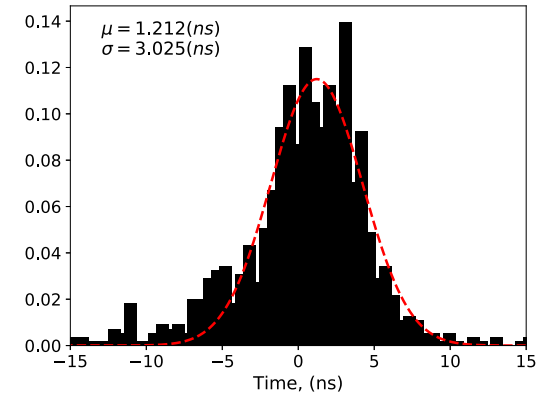

(a) The time difference between the TRIGGER and CONFIRM stations signals (after correcting for the time of flight between the two stations).

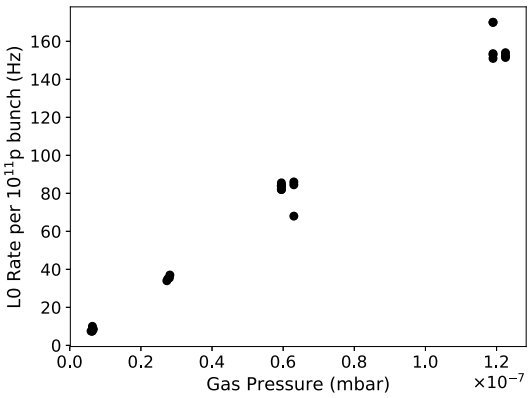

(b) Dependence of the L0 trigger rate on the pressure inside the gas target chamber.

FIG. 3. Trigger system performance.

The ghost charge fraction (the fraction of protons in LHC bunch slots that are nominally empty) can also be measured

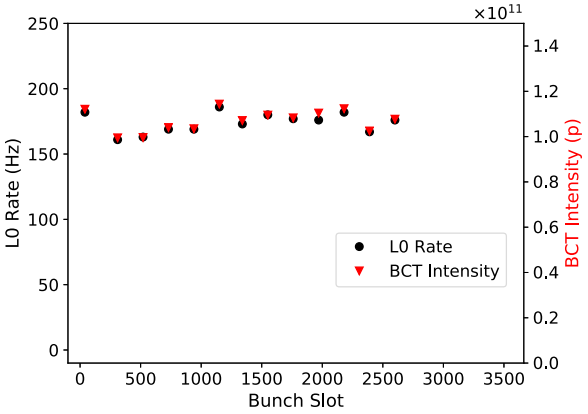

FIG. 4. The BGV $L0$ trigger rate per bunch for an LHC fill with 13 bunches (circles) and an independent measurement of the bunch populations made with the LHC BCT system (rectangles, with values referring to the scale on the right).

by performing similar rate measurements both with and without injecting gas. From such data, the total ghost charge fraction for a typical LHC fill is measured to be around $(1.0 \pm 0.1)\%$. Through such measurements, the background contamination of the $L0$ trigger is measured to be at the level of 0.1%.

IV. SCINTILLATING FIBER TRACKING DETECTOR

A. Detector design and construction

The BGV tracking detector is located outside the LHC beam vacuum and has no movable parts (see Fig. 1). The detector design is optimized for the (i) maximal geometric acceptance, (ii) minimal distance to the beam line, in order to reduce the track extrapolation uncertainty to the beam-gas interaction vertex, (iii) sufficient granularity for adequate pattern recognition in the LHC environment while minimizing the number of readout channels (for simplicity and cost reasons), and (iv) minimal number of tracking planes to reduce costs.

The BGV tracking detectors are large scintillating fiber planes providing a hit resolution of better than 100 μm, that are read out using silicon photomultipliers (SiPMs). Taking into account the kinematic properties of the beam-gas interaction products, the detector is designed to cover polar angles in the range from 10 to 100 mrad over more than 1 m in length (along the z axis) of the interaction region.

The detector system comprises two tracking stations, the *near* and *far* stations as shown in Fig. 1. Both stations consist of four double-sided scintillating fiber modules, with each module providing two one-dimensional measurements of the particle position. On the front face of each module, the fibers are oriented vertically (X plane), while on the back face the fibers are inclined by 2° (X' plane) to facilitate the pattern recognition. Each SciFi module has an active area of 260 mm × 340 mm with a 97 mm × 97 mm cutout at one corner, which allows a better azimuthal acceptance to be achieved.

The modules consist of two detection planes, each made of four or five layers of scintillating fibers. Four-layer mats are used in the near station to minimize the radiation length and, therefore, the multiple scattering caused by the modules. Two consecutive modules are placed with a relative angle of 90° in each top and bottom part of a station. A four-coordinate measurement (X, X' and Y, Y') is therefore made per passing particle.

In order to get the maximum polar angle coverage given the constraints imposed by the adjacent LHC beam 1 vacuum tube, the BGV detector is built out of two sets of SciFi modules, one above (top) and one below (bottom) the LHC beam vacuum pipe. The overlap region between the top and bottom modules (an area of about 20 mm × 20 mm) can be used to improve the relative alignment of the modules.

The fiber mats for the BGV detector were produced following the procedure used for the LHCb SciFi tracker upgrade [14]. The active material is a round, double-cladded 0.25-mm-diameter plastic scintillating fiber, produced by Kuraray (Japan). Consecutive fibers and fiber layers are interleaved with epoxy glue for mechanical stability, with the optical cross talk between the fibers eliminated by adding TiO_2 powder to the glue mixture. Four or five fiber layers, each 65 mm wide, form one fiber mat, corresponding to one active plane.

A mirror foil is glued at the extremity of the fibers (edge of the module) in order to maximize the light collection. The scintillation light is detected by 128-channel SiPM arrays of type Hamamatsu H2014 [15], containing 104 pixels per channel. Each fiber plane is read out by eight SiPM arrays (1024 channels), such that the full detector system comprises 128 SiPM arrays (16 384 channels).

All elements of a SciFi module (fiber mats, Rohacel support, cooling enclosure, front-end electronics, and alignment references) are attached to a solid plastic plate. The material budget of a module is (in radiation lengths, x/X_0) 0.94% and 1.05% for four- and five-layer mats, respectively, with the fibers accounting for 0.56% and 0.67%.

B. BGV operation in the LHC radiation environment

The BGV sensors and front-end electronics are exposed to background radiation generated by beam losses and beam-gas interactions. Radiation damage leads to an increase in the optical attenuation of the scintillating fibers, but the effect on the detector performance is insignificant due to the small size of the modules. On the other hand, the neutron fluence increases the SiPM dark count rate [14], which necessitates cooling of the SiPMs in order to maintain an acceptable noise cluster rate [16,17].

The expected radiation fluence and dose can be estimated from the predicted rate of beam-gas interactions, giving a yearly charged particle fluence of 4×10^{10} cm^{-2} in the region of the BGV tracker. This is the integrated fluence at radii between 22 and 26 cm around the LHC beam pipe, where the BGV tracker sensors are located. Since most charged particles are highly energetic (more than 1 GeV), this fluence can be translated into about $2 \times 10^{10} n_{\mathrm{eq}}$ cm^{-2} (where n_{eq} stands for "1 MeV neutron equivalent") and to a dose of the order of 1 Gy/yr.

A single phase cooling system is installed to cool down the SiPMs. A brief overview of the system is given here, while a more detailed description can be found in Refs. [16,17]. The cooling system is composed of a commercial refrigerator unit located in the service tunnel and cooled by ambient air. This is operated in a closed loop with C_6F_{14} fed into a pair of 25-m-long transfer lines before reaching the main manifold located inside the LHC tunnel. The manifold provides four parallel output loops for

detector cooling, each individually tunable by a manual needle valve. C_6F_{14} is chosen for both its thermal properties and radiation resistance. The power dissipation per module has been measured to be approximately 20 W (dominated by heat leaks).

A typical flow of 20 $1\,\mathrm{min}^{-1}$ with a supply temperature of $-15\,°\mathrm{C}$ at the refrigerator is used to achieve a detector temperature of approximately $-10\,°\mathrm{C}$. The refrigerator's control system keeps the cooling fluid temperature stable within less than 0.1 °C. Temperature variations between different SiPMs are also measured to be less than 0.1 °C. The SiPM cold boxes as well as the main manifold are flushed with dry air in order to prevent water vapor condensation.

C. Detector metrology and alignment

Care has been taken to accurately position the BGV detector modules in order to provide a good starting point for the software track reconstruction. The detector alignment steps are summarized in this section, while further details can be found in Refs. [16,18].

1. Single-module metrology

Measurements were performed in the laboratory for each detector module in order to determine the actual dimensions and exact position of the active detector planes and the alignment targets installed on each module. The results showed that the module geometry was in good conformity to the design [16]. The angle between the two active planes in each module was measured to be in the range 1.9°–2.1°.

2. Two-module assemblies

The modules were paired and assembled together in the lab using a common "detector plate" and assembled using the single-module metrology data to adjust their positions. Alignment targets fixed on the detector plates could then be used in the tunnel for final alignment of the two-module assemblies. Using the available metrology data, a mechanical model was constructed to allow the position of the module edges to be estimated from these alignment targets.

3. Installation and alignment of two-module assemblies in the LHC tunnel

The two-module assemblies were fixed onto the detector support frame in the LHC tunnel using prealigned fixation plates. Survey measurements of the alignment targets of the two-module assemblies were used to adjust the angular position of the detector modules. In parallel, the two-module assemblies were translated such that the detector modules approached the vacuum chamber wall to within 0.3 mm.

V. DATA ACQUISITION, CONTROL, AND ON-LINE PROCESSING SYSTEM

The control and readout system of the BGV detector is largely based on that of the LHCb vertex locator (VELO) detector [19] and is described in detail in Ref. [20].

The detector is configured and monitored through dedicated control computers, using software based on the LHCb detector control system [21,22]. The fast signals (*L*0 trigger, clock, and test pulse trigger) are orchestrated by the LHCb readout supervisor board (ODIN), which distributes the necessary signals to the front-end electronics, while the high-level trigger (HLT) runs on a dedicated CPU farm that performs the event filtering and reconstruction. This farm performs as well on-line data analysis for real-time beam size measurements.

A. Readout electronics chain

The SiPM output signals are read out with the radiation-tolerant Beetle front-end chip developed for LHCb [23]. In each Beetle chip, 128 channels are sampled synchronously with the 40 MHz LHC bunch arrival clock. On reception of a trigger, each Beetle chip sends the analogue data of the corresponding clock cycle on four output ports. There are 32 channels per port, time multiplexed at 40 MHz. Analogue front-end BGV data can thus be transmitted for digitization at a maximum rate of 1.1 million events per second.

Since the Beetle chip is designed to operate with relatively small input signals [on the order of 10^4 electrons per minimum ionizing particle (MIP)] from silicon strip detectors, the BGV front-end electronics contain an attenuator for each channel in order to adapt the SiPM signals (on the order of 10^7 electrons per MIP) to the Beetle dynamic range. This is based on an *RC* circuit providing an attenuation factor of about 300. The analogue, time-multiplexed data of a SciFi module are read out by 16 Beetle chips and sent to a repeater board (RPT), situated a few meters away from the detector. There is one RPT per module. The RPTs buffer the Beetle data and drive them over 60 m of cable to the BGV readout boards (TELL1, developed for LHCb [24]) situated in the LHC service tunnel, away from radiation.

The low-voltage and SiPM bias-voltage systems are built from commercial components. A single mainframe houses five low-voltage and one bias-voltage supply cards. The 32 bias-voltage channels available are used to set a common voltage on groups of four SiPM arrays.

B. On-line zero suppression

Zero suppression is achieved in two steps. First, the raw signals are corrected for noise introduced in the readout chain, and then a threshold-based algorithm is applied to combine signals from adjacent channels to suppress the dark counts from SiPMs and so reduce the

data rate. These operations are performed on-line in the TELL1 readout boards. This section gives an overview of this process, with more details available in Refs. [25,26].

1. Raw data corrections

Extensive studies of all noise and signal distortions introduced in the readout chain have been performed for the LHCb VELO detector [27,28]. The VELO correction algorithms implemented in the data processing field-programmable gate array of the TELL1 were adapted for use by the BGV. The noise is dominated by three sources: pedestal fluctuation from random electronic noise, header cross talk (cross talk in the multiplexed Beetle output ports), and common mode noise (baseline shift on an event-per-event basis for all channels of an analogue link).

A channel correlation correction is applied which mitigates cross talk between channels that originates in the front-end board (signal routing between SiPMs and Beetle chips). For a given channel i, the signal amplitude $A(i)$ is corrected by subtracting a fraction $x_{j\to i}$ of the signal amplitude of a neighboring channel j. Laboratory measurements have shown that the most significant correlations (above 10%) come from channels $j = i + 3$ and $j = i + 5$, and, therefore, only those are corrected for:

$$A_{\text{corrected}}(i) = A_{\text{raw}}(i) - x_{i+3\to i}A_{\text{raw}}(i+3) - x_{i+5\to i}A_{\text{raw}}(i+5). \quad (2)$$

2. Clustering

A threshold-based algorithm is implemented after the raw data corrections that combines neighboring channels to form *clusters*. The algorithm comprises three steps [29] and is illustrated in Fig. 5: (i) Identify channels with a signal amplitude above a *seed threshold* (seed channels), (ii) identify channels with a signal amplitude above a *neighbor threshold* (neighbor channels), and (iii) form clusters from adjacent seed channels and, at most, one neighbor channel on the left and one on the right (total size limited to four channels). Retain only the clusters with total signal amplitude above a given *sum threshold*.

The cluster position is encoded in 14 bits: 11 bits that identify the reference channel of the cluster within the module and a relative offset encoded in three bits, corresponding to a precision of 31 μm.

The clustering thresholds are optimized to provide a high detection efficiency while keeping the noise rate at an acceptable level. To obtain a uniform response, the seed and neighbor thresholds can be adjusted for each channel separately, while the sum threshold can be adjusted for groups of 64 channels. We chose to adjust the thresholds per SiPM array (128 channels) to provide a uniform distribution of noise clusters from the SiPM dark counts. Under the nominal 2017 operating conditions (SiPMs at $T = -10\,°\text{C}$ and overvoltage $\Delta V = 3.5$ V), the seed thresholds were set in the range 1.5–2 photoelectrons in order to obtain a cluster detection efficiency above 98% and, on average, only 1.5 noise clusters per module per event.

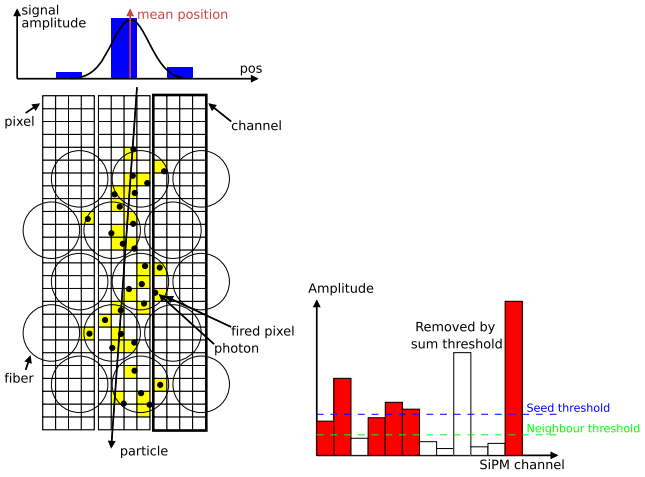

FIG. 5. Left: Signal formation in a SciFi module. Scintillation photons are detected by several SciFi fibers, triggering pixels of the SiPM. Only the sum of signals from the 104 pixels within a SiPM channel is read out. A weighted average is used to measure the exact coordinate of a cluster. Right: Illustration of the clustering algorithm and thresholds.

The correction algorithm is calibrated in the laboratory, tested on non-zero-suppressed data and implemented in the BGV TELL1 boards [30].

C. BGV control system

The BGV detector control system is described in detail in Ref. [20]. It is based on the WinCC SCADA (supervisory control and data acquisition) software. On this base software layer, a CERN-wide framework (the Joint Controls Project) is added. It runs on a dedicated Linux computer in the LHC service tunnel. An additional computer, the CAN router, is used for CAN (controlled area network) bus communication with components that use the open platform communications protocol. This is used to control the voltage supply to the SiPM arrays and Beetle readout chips and to acquire data from the SiPM temperature sensors.

The ODIN readout supervisor board [31] receives the LHC clock and $L0$ trigger decision and coordinates the overall data acquisition. The clock, which is received by all readout components, serves as a metronome and can be adjusted in several places to allow for corrections due to the different signal propagation times in the system.

D. High-level trigger

The detector front-end boards send analogue data to the TELL1 readout boards for digitization and clustering. The data processing time on the TELL1s depends on the number of clusters found. Hence, the buffer is protected by a trigger rate control network that moderates the readout

sequence. The TELL1 boards are connected to a CPU farm through a network with a bandwidth of approximately 200 MB s^{-1}, which can sustain an event transfer rate of up to 500 kHz. The BGV readout system uses the LHCb VELO data format [30].

The BGV HLT system currently consists of five servers hosted in an HP Blade system. First, a quick selection is made based on the cluster multiplicity per detector module (two detector planes). At least two clusters per module are required, corresponding to a minimum of two detected tracks. An upper limit of 50 clusters per module is used to limit the subsequent processing time. This simple selection enhances the fraction of events processed with at least two reconstructed tracks from 7% to 56%. Subsequently, a track reconstruction algorithm is run on the events passing the cluster multiplicity selection. The flexibility of the HLT allows additional event selection criteria to be applied and a choice of the fraction of events to be stored for further analysis. Events are stored off-line at a maximum rate of 10 kHz. They are analysed by the HLT system at the same rate to provide real-time beam size measurements.

VI. SCIFI DETECTOR PERFORMANCE

A four-layer BGV fiber module was tested in the experimental setup of the LHCb SciFi tracker test beam at the CERN Super Proton Synchrotron. The setup included a telescope, placed approximately 20 cm upstream of the BGV module, used to reconstruct the tracks of particles. It consisted of five tracking stations made of short scintillating fiber mats, where each station provided a two-dimensional position measurement in the transverse plane. The cluster resolution of each detection plane of the telescope was 33 μm, which resulted in a resolution of the impact point on the BGV module, after extrapolation, $\sigma_{\text{track}} = 45$ μm. This section describes the measurement of the most important module performance characteristics. More details can be found in Refs. [26,32].

A. Light yield

The total amount of light detected from a crossing particle is the main parameter that influences the cluster detection efficiency. Random fluctuations associated with the energy deposition of charged particles in matter (Landau distributed for a thin layer) give rise to a spread in the intensity of the detected light signals. In addition, the energy deposited by a particle in the fiber mat can be distributed over several readout channels which need to be combined to form *clusters* using the threshold-based algorithm described above. The *cluster sum* is the total amount of signal per cluster.

The distribution of the cluster sum measured for each detection plane at the nominal SiPM bias overvoltage ($\Delta V = 3.5$ V) is shown in Fig. 6. The result is expressed in photoelectron (PE) units which represent the amount of signal produced by a single photon. The light yield, defined as the most probable value of the distribution, is found to be 15.6 and 14.6 PE, respectively, for the X and X' planes of the module.

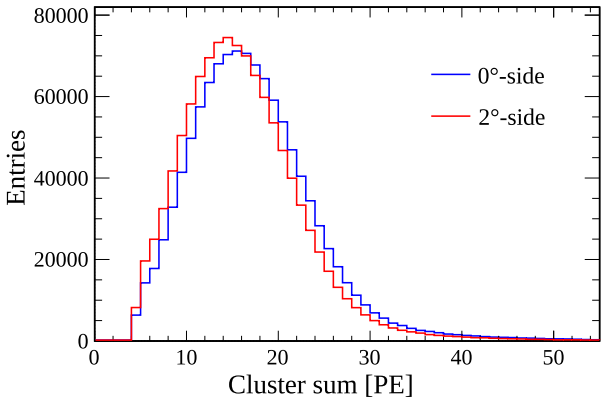

FIG. 6. Cluster sum distribution in the two detection planes of a four-layer BGV SciFi module. The measurement was performed with the nominal SiPM overvoltage $\Delta V = 3.5$ V.

Depending on the beam spot position, the light yield was seen to vary between 13 and 18 PE. These variations were attributed to the longitudinal position of the hit in the fiber (10% light yield difference from attenuation between the top and bottom of the fibers), the nonuniformity in the fiber mat quality, and the temperature of the SiPMs (which for the test was not stabilized, leading to a 10% effect on the photon detection efficiency). However, these variations do not impact the hit detection efficiency, as the amount of signal remains above the clustering thresholds.

For five-layer modules, the low light signals (below 10 PE) have amplitudes that are higher by 20% due to the additional light collected in the extra fiber layer. As a consequence, the cluster detection efficiency is higher for these modules. The expected improvement is smaller for hits with a high signal amplitude, due to signal saturation in the front-end board.

B. Cluster detection efficiency

The cluster detection efficiency $\varepsilon_{\text{cluster}}$ is calculated as the ratio of the number of events with a cluster detected at a small distance (seed distance) from the actual impact point of the track (as determined by the telescope) to the total number of events. A seed distance of 1.25 mm is used in order to include tracks with large scattering angles. The average module cluster detection efficiency is $\varepsilon_{\text{cluster}} = (98.0 \pm 0.4)\%$ using clustering thresholds (seed/neighbor/sum) of 2.5/1.5/4.5 PE and $(98.7 \pm 0.4)\%$ with the threshold lowered to 1.5/0.5/2.5 PE. Approximately 2% of the nominally sensitive area of the SciFi modules is inefficient due to construction constraints (space between adjacent SiPMs, imperfect positioning, or longitudinal cuts fiber mats, etc.).

C. Single-cluster spatial resolution

The spatial resolution σ_{cluster} is calculated from the residual between the cluster detected on the module and the impact point of the track. The distribution of residuals is the convolution of the cluster and track position resolutions ($\sigma^2_{\text{residual}} = \sigma^2_{\text{cluster}} + \sigma^2_{\text{track}}$). Using the nominal seed, neighbor, and sum thresholds of 2.5, 1.5, and 4.5 PE, respectively, the cluster resolution σ_{cluster} is estimated to be (38 ± 3) μm for the X and (43 ± 4) μm for the X' detection plane, given the performance of the tracking telescope used.

VII. TRANSVERSE BEAM SIZE MEASUREMENT METHOD

The transverse beam profiles may be obtained by producing distributions of beam-gas interaction vertex positions, each vertex being reconstructed from several tracks of the triggered event. However, this method requires a stand-alone precise estimation of the tracker performance, in particular, of the vertex position resolution. For the sake of simplicity, rapidity, and cost, the BGV system comprises only the minimum set of detector planes required to reconstruct tracks (i.e., two for each coordinate). An alternative method to measure only the beam size (the standard deviation of the transverse beam profile), without relying on vertex distributions, is presented here. This makes use of only reconstructed tracks, by exploiting correlations in their impact parameter (IP, defined in Sec. VII D) relative to the primary vertex. All results presented here are obtained using this IP correlation method.

A. Track reconstruction and event selection

High-energy particles emerging from the beam-gas interaction region travel straight through the BGV detector as there is no sizable magnetic field in the vicinity of the setup. Their trajectories can therefore be reconstructed as straight lines using the one-dimensional position of reconstructed clusters in all the SciFi planes. As the detector has two identical parts (top and bottom), the track reconstruction can be performed separately for each of them. Special care is taken to avoid double counting of tracks that go through the overlap region between the top and bottom parts.

The track pattern recognition algorithm starts from a seed in the first plane of the far SciFi detector station from which searches are made for suitable combinations in the other modules along the possible particle direction (by defining appropriate search windows). Given the track multiplicity expected per beam-gas interaction (up to about ten tracks) and the fact that the SciFi detectors perform one-dimensional measurements, the number of possible tracks exceeds the number of real particles. All reasonable cluster combinations are evaluated in order to select good quality tracks that point to the interaction region. The reconstruction step sequence is as follows.

Track seed.—A cluster is selected in the first plane of the far station and combined with a cluster in the corresponding plane of the near station to form a seed track. If the seed track does not point to the gas target volume, the cluster combination is rejected.

Pattern recognition.—The pattern recognition algorithm used is a process that scans sequentially through all detector planes (downstream to upstream) for clusters that might be associated together to form a track. Initially, the seed track clusters are used to define a search window in the second downstream detector plane (the first one being already used for the definition of the track seed). If in that window there is an available cluster (not associated with another track), it is included in the cluster list of the track under study. The search is then repeated for the next detector plane. Each time, the full current cluster list is used to define the search window. This procedure is terminated when a track with a cluster in each of the eight planes is identified.

Track fit.—A linear fit is performed using the coordinates of the eight clusters of a given track. If the χ^2 of the fit is below a certain limit, the clusters found are grouped into a cluster set (corresponding to a track) and marked as "used" (not available for any other possible cluster set). The procedure then restarts with the next cluster available at the first plane of the far station.

Once a full list of cluster sets is established, a linear fit to each of them provides the corresponding final track parameters (point of closest approach to the z axis, directional vector, χ^2, and covariance matrix).

Simulation studies show that up to 30% of reconstructed tracks may not correspond to real particles traversing the detector. This is mainly due to background cluster combinations that cannot be eliminated due to the limited number of tracking planes. Figure 7(a) shows the multiplicity of reconstructed tracks for real data and Monte Carlo (MC) simulated p-Ne interactions. Figure 7(b) shows the tracking efficiency and purity from the simulation. Efficiency is defined as the fraction of reconstructed tracks generated from particles leaving one MC hit in each of the eight planes of one BGV detector half, top or bottom (reconstructible tracks). Purity is defined as the fraction of reconstructed tracks that are associated with a reconstructible particle.

B. Alignment of detector elements

In order to obtain precise results from the track fit procedure described above, the exact position of the various detector elements needs to be known. Even though all detector planes are installed very close to their nominal position, some corrections still need to be introduced in the off-line analysis.

Once track fit results are obtained for a given data sample, the mean value per plane of the cluster residuals

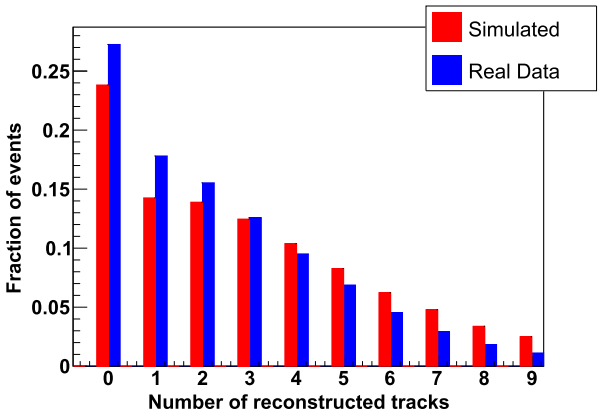

(a) Reconstructed track multiplicity.

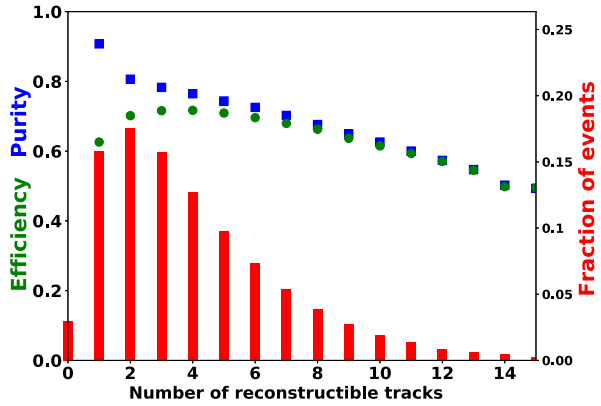

(b) Track reconstruction efficiency (green disks) and purity (blue squares) together with the reconstructible track multiplicity (red bars).

FIG. 7. Performance of the track reconstruction algorithm.

(distance between clusters and the fitted line) indicates systematic shifts. For offsets within individual modules of the detector, the corresponding corrections are directly inserted in the relevant database used for track fitting.

In order to select a subsample of reconstructed tracks that point to the interaction region, a simple vertex finding algorithm is used. Using the fact that the beam-gas interaction region is over a meter long along the z axis, a relative transverse misalignment between BGV SciFi modules results in a slope of the reconstructed vertex position along the z axis. Such slopes are then corrected by introducing relative shifts between the detector modules. In that way, the top and bottom modules are independently aligned. As a final step, the complete detector is shifted in order to reconstruct a beam spot centered around the beam axis. All these alignment corrections are used for the results presented here.

C. Estimation of the transverse beam position

The signed IP d is defined here as the distance of closest approach between a track projected in the x-y plane and (0,0). It is given by

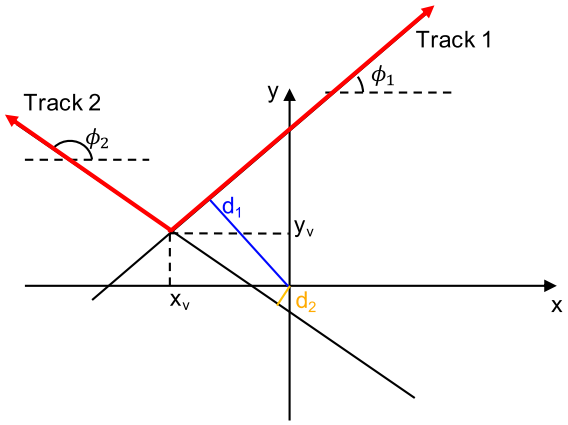

FIG. 8. Two tracks from the same vertex (red lines), with their corresponding d and projected azimuth angle. The arrows indicate the direction of particles emerging from the beam-gas interaction vertex through the BGV detector.

$$d = x\sin\phi - y\cos\phi, \tag{3}$$

where (x, y) is any point along the track and ϕ its azimuth angle (Fig. 8). Assuming all tracks share a common vertex point (x_v, y_v), Eq. (3) can be used to determine the transverse position of the beam, by fitting the distribution of d_v for all angles. This is shown for a typical data sample in Fig. 9. A fit using (x_v, y_v) as free parameters then provides the transverse position of the beam with respect to the center of the BGV. Figure 9(a) shows the distribution before any alignment correction is applied, while the distribution for the same data sample, after the alignment corrections, is shown in Fig. 9(b). The plots presented are for 100 000 events (the number of entries indicated corresponds to the number of reconstructed tracks in each case). Applying the alignment correction, the number of reconstructed tracks is increased by 15%. The beam spot is reconstructed at $(x_v, y_v) = [0.015(3)\ \text{mm}, -0.025(3)\ \text{mm}]$, demonstrating the effectiveness of this alignment procedure.

D. Impact parameter correlation method

The IP of tracks from particles generated by beam-gas interactions can also be used to measure the transverse beam size of a beam centered around the z axis. For previous applications of this method, see Refs. [33,34].

For each interaction vertex, the IPs of the emerging tracks are correlated. Using Eq. (3) at (x_v, y_v), this correlation can be written as

$$\begin{aligned} d_1 d_2 &= (x_v\sin\phi_1 - y_v\cos\phi_1)(x_v\sin\phi_2 - y_v\cos\phi_2) \\ &= \frac{1}{2}(x_v^2 + y_v^2)\cos(\phi_1 - \phi_2) \\ &\quad - \frac{1}{2}(x_v^2 - y_v^2)\cos(\phi_1 + \phi_2) \\ &\quad - x_v y_v \sin(\phi_1 + \phi_2). \end{aligned} \tag{4}$$

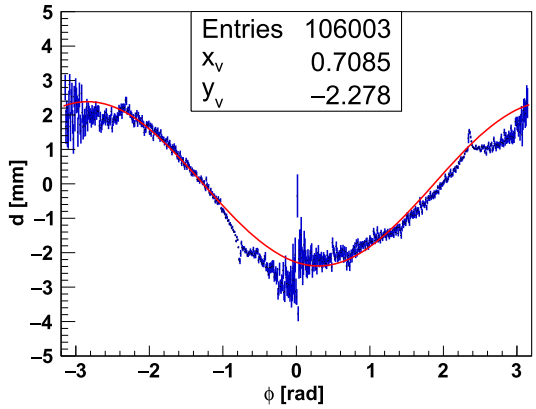

(a) d vs ϕ distribution before alignment correction.

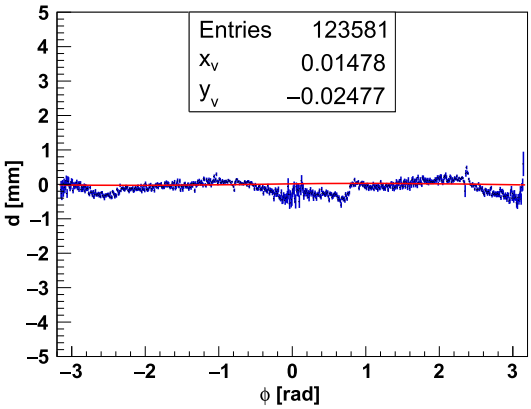

(b) d vs ϕ distribution after alignment corrections

FIG. 9. Estimation of the transverse beam spot position with the BGV detector. Red lines are the result of a fit with Eq. (3) estimating the beam spot position (x_v, y_v).

For any given value $(\phi_1 - \phi_2)$, the average correlation $\langle d_1 d_2 \rangle$ can be, using Eq. (4), written as

$$\langle d_1 d_2 \rangle|_{(\phi_1-\phi_2)} = \frac{1}{2}(\langle x_v^2 \rangle + \langle y_v^2 \rangle)\cos(\phi_1 - \phi_2), \quad (5)$$

assuming uncorrelated vertex coordinates (i.e., $\langle x_v y_v \rangle = 0$) and uniformly distributed ϕ_1 and ϕ_2 [i.e., $\langle \cos(\phi_1 + \phi_2) \rangle = 0$]. Brackets indicate an average over many track pairs. Track pairs are formed within the same triggered event and accumulated over many triggers.

Given that $\langle x_v \rangle = 0$ and $\langle y_v \rangle = 0$, $\langle x_v^2 \rangle$ and $\langle y_v^2 \rangle$ are the variances σ_x^2 and σ_y^2 of the transverse beam spot, in the x and y direction, respectively. Equation (5) can then be rewritten as

$$\langle d_1 d_2 \rangle|_{(\phi_1-\phi_2)} = \frac{1}{2}(\sigma_x^2 + \sigma_y^2)\cos(\phi_1 - \phi_2). \quad (6)$$

Similarly, by expanding Eq. (4) for a fixed $(\phi_1 + \phi_2)$ value, one gets

$$\langle d_1 d_2 \rangle|_{(\phi_1+\phi_2)} = \frac{1}{2}(\sigma_x^2 - \sigma_y^2)\cos(\phi_1 + \phi_2). \quad (7)$$

It should be noted that the average IP correlation is independent of the IP measurement resolution. By adding a random error ϵ to each measurement, one gets

$$\langle (d_1 + \epsilon_1)(d_2 + \epsilon_2) \rangle = \langle d_1 d_2 \rangle + \langle d_1 \epsilon_2 \rangle + \langle d_2 \epsilon_1 \rangle + \langle \epsilon_1 \epsilon_2 \rangle.$$

Assuming statistical independence between errors and measurements, $\langle d_i \epsilon_j \rangle = \langle d_i \rangle \langle \epsilon_j \rangle$ and $\langle \epsilon_1 \epsilon_2 \rangle = \langle \epsilon_1 \rangle \langle \epsilon_2 \rangle$, giving $\langle (d_1 + \epsilon_1)(d_2 + \epsilon_2) \rangle = \langle d_1 d_2 \rangle$ (provided the measurements do not introduce any systematic bias, $\langle \epsilon \rangle = 0$). Therefore, by using Eqs. (6) and (7), the transverse beam size can be directly measured, without having to correct it for the IP (i.e., tracking) resolution. This is valid only for tracks originating from the primary vertex. The achievable transverse beam size measurement precision still depends on the IP resolution, as this determines the number of background tracks that are wrongly identified as originating from the primary vertex.

VIII. LHC BEAM 2 SIZE MEASUREMENTS

The impact parameter correlation method can be used to measure the transverse size of the LHC beam. During the 2018 LHC operation period, several beam size measurement campaigns were performed using the BGV detector. Events were first selected using the following criteria: (i) $2 <$ number of clusters per detector plane < 50, (ii) reconstructed tracks with a hit in each of the eight detector planes, (iii) track fit $\chi^2 < 100$ per track, (iv) tracks with a reconstructed point of closest approach to the z axis (beam direction) inside the BGV gas target volume, and (v) correlations calculated only for track pairs with their points of closest approach closer than 40 mm along the z axis.

Figure 10 shows the distribution of the IP correlation as a function of $\cos(\phi_1 - \phi_2)$ (a) and $\cos(\phi_1 + \phi_2)$ (b) for a sample of 500 000 tracks recorded during stable operation period at 450 GeV. Each of these two distributions is fitted with a straight line. Based on Eqs. (6) and (7), the line slope in Fig. 10(a) is an estimator of $\frac{1}{2}(\sigma_x^2 + \sigma_y^2)$ and that of Fig. 10(b) of $\frac{1}{2}(\sigma_x^2 - \sigma_y^2)$, from which the horizontal and vertical beam size, σ_x and σ_y, respectively, can be obtained.

A. Beam size estimation and simulation-based correction

The transverse beam size measurement method described above was first studied with MC events. The detector simulation was derived from the LHCb simulation framework using GEANT4 [35]. It is based on a detailed description of all the detector elements and on the heavy ion jet interaction generator (HIJING) model for generating p-Ne interactions [36]. Real data and MC predictions are compared in Figs. 11 and 12. The fine structure of the distributions is well described by the BGV simulation. The real data excess at $z < 0$ in Fig. 12 comes from

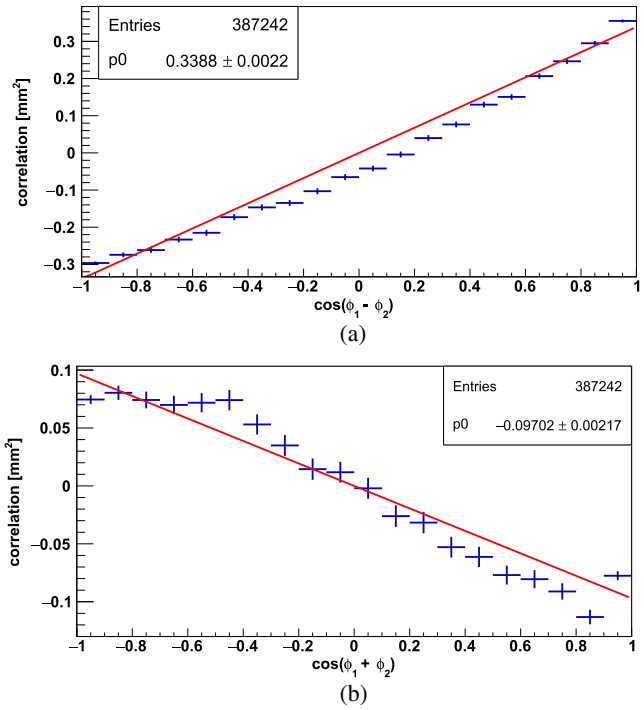

FIG. 10. IP correlation vs $\cos(\phi_1 - \phi_2)$ (a) and $\cos(\phi_1 + \phi_2)$ (b). From the two line slopes and Eqs. (6) and (7), one gets for the transverse beam size $\sigma_x = 660$ μm and $\sigma_y = 492$ μm.

interactions upstream that miss the veto trigger scintillator and are not considered in the BGV simulation.

Several MC datasets were studied, each with a different simulated beam size. For each sample, tracks were reconstructed in the same way as for real data. Each reconstructed beam size σ^{rec} is compared with the original, used for the generation of the MC data, σ^{MC}.

The reconstructed beam size always underestimates the true beam size. Furthermore, this underestimation is not the same for the measurement along the x and y axes. These effects are attributed to two main factors. First, the detector coverage is not z-axial symmetric. Second, background

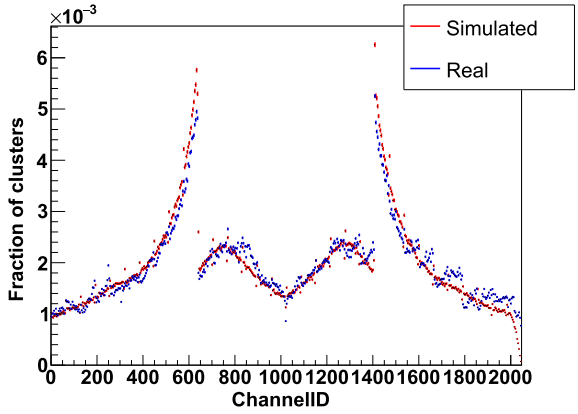

FIG. 11. Measured (blue points) and MC simulated (red points) SciFi cluster distribution along a SciFi module.

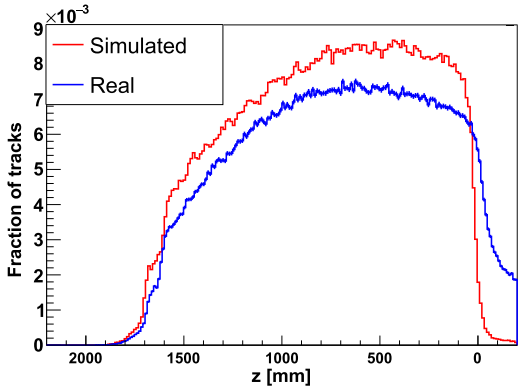

FIG. 12. The distribution of the point of closest approach of reconstructed tracks along the z axis (beam direction), for real data and MC simulation predictions.

hits induce a number of wrongly reconstructed tracks due to the limited number of tracking planes. These wrongly reconstructed tracks have no correlation between the IP and azimuth angle. This results in the corresponding data points in the IP correlation distribution as a function of $\cos(\phi_1 - \phi_2)$ or $\cos(\phi_1 + \phi_2)$ being evenly distributed around 0 for both variables. Their use in the linear fits in Fig. 10 therefore produces a line with a smaller slope, resulting in a smaller reconstructed beam size. Figure 13 shows σ^{MC} vs σ^{rec} for both the horizontal and vertical transverse beam sizes. By fitting a second-order polynomial to these data, a correction function is obtained that converts the raw reconstructed measurements to a final, corrected beam size estimations (σ^{cor}):

$$\sigma_x^{\mathrm{cor}} = 0.81(\sigma_x^{\mathrm{rec}})^2 + 0.53\sigma_x^{\mathrm{rec}} + 0.07 \quad \text{and}$$
$$\sigma_y^{\mathrm{cor}} = 1.39(\sigma_y^{\mathrm{rec}})^2 + 0.72\sigma_y^{\mathrm{rec}} + 0.06. \tag{8}$$

These parameters are used to obtain beam sizes from real data.

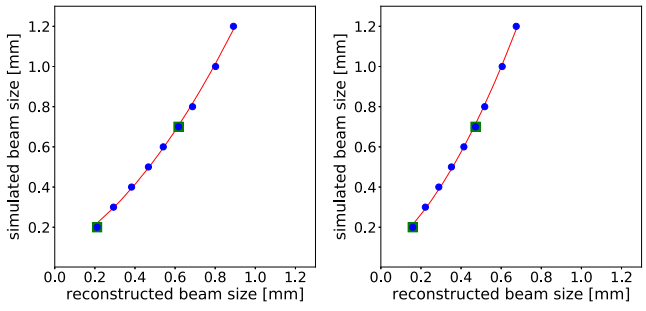

(a) σ_x^{MC} vs σ_x^{rec} (b) σ_y^{MC} vs σ_y^{rec}

FIG. 13. Reconstructed beam size σ^{rec} plotted against the corresponding MC generated beam size σ^{MC}. The red line is a quadratic fit to the data. The two green squares are beam size estimations for two additional MC samples that were not used in the line fit.

B. Beam size measurements at stable energies

During stable LHC operation at collision energy with protons, the beam emittance and, hence, beam size remain practically constant. These are ideal conditions to study the BGV detector performance. Acquiring data for an extended period (of the order of 30 min) allows a straightforward estimation of the statistical error of the BGV measurements.

Using all the events within a time slice of a given duration (integration time), an IP correlation vs $\cos(\phi_1 - \phi_2)$ [and $\cos(\phi_1 + \phi_2)$] distribution is obtained, and the corresponding beam size is estimated [using Eq. (8)]. Consecutive time slices provide independent measurements of the same, stable, beam size.

During the LHC fill no. 7314 (2556 proton bunches per beam, 1.2×10^{11} protons per bunch, 4.3×10^{-8} mbar Ne pressure in the BGV target chamber, and 4.9 kHz BGV readout rate, 17 October 2018), such a dataset was acquired with the results presented below.

Figure 14 shows the distribution of the transverse beam size for two integration times. The measurements are seen to be normally distributed; hence, the statistical error of the BGV measurement for each integration time can be estimated from the width of the corresponding normal distribution. The resulting errors scale with the number of analyzed events as $N^{-1/2}$. This allows the statistical error of a BGV measurement to be calculated based on the integration time (or, equivalently, the number of events used). Typical BGV beam size measurements with their corresponding errors are presented in Table I.

Figure 15 shows a comparison of the transverse beam size measured by the BGV and that using the LHC synchrotron radiation telescope (BSRT) [37] for various beam energies. It should be noted that the BSRT is located at a different position in the accelerator than the BGV. Hence, a good knowledge of the beta functions (β_x, β_y) is required to scale the beam size from one location to the other. These are typically known with a precision of better than 5% [38].

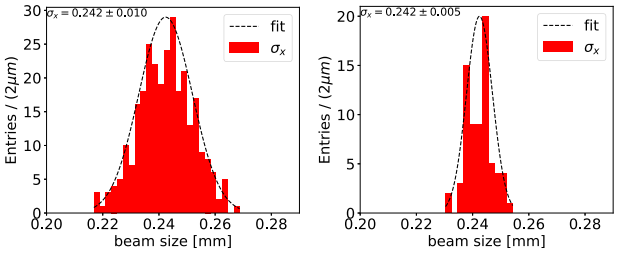

(a) 5 s integration time. (b) 20 s integration time.

FIG. 14. Distribution of independent beam size measurements for two integration times. Black lines are fits with a normal distribution, whose width reflects the statistical error of the BGV beam size measurement.

TABLE I. BGV transverse beam size measurements for various LHC beam energies (i.e., beam sizes) and integration times. For each energy, all estimates for the various integration times use the same data sample.

Integration time (s)	Beam energy (TeV)	σ_x (μm)	σ_y (μm)
5	0.45	814 ± 15	772 ± 15
20	0.45	815 ± 8	772 ± 8
80	0.45	815 ± 4	772 ± 4
5	2.50	419 ± 13	420 ± 13
20	2.50	419 ± 7	420 ± 7
80	2.50	419 ± 3	421 ± 3
5	6.50	242 ± 10	223 ± 10
20	6.50	242 ± 5	223 ± 5
80	6.50	242 ± 2	223 ± 2

C. Measurements during the LHC proton acceleration phase

As shown in the previous section, accurate transverse beam size measurements can be obtained with relatively short integration times (10–20 s). The BGV detector can therefore also be used to measure the beam size as it evolves during the acceleration phase of the LHC cycle, which typically lasts about 20 min. Figure 16 shows the results for one LHC cycle (fill no. 6428, 28 November 2017). Here, the measured beam size from the BGV is

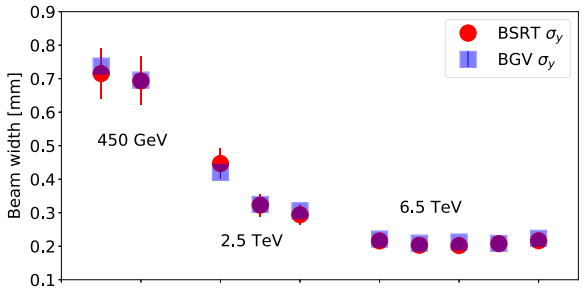

FIG. 15. Transverse beam size measurements for the BGV (blue squares) and BSRT extrapolated to the BGV location (red circles) for three different beam energies.

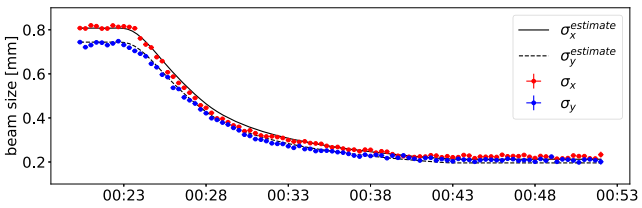

FIG. 16. BGV measurement of transverse beam size during the LHC acceleration phase. The expected beam size evolution given by Eq. (9) is also drawn. For clarity, the symbols used per data point are larger than the error bars of the measurements.

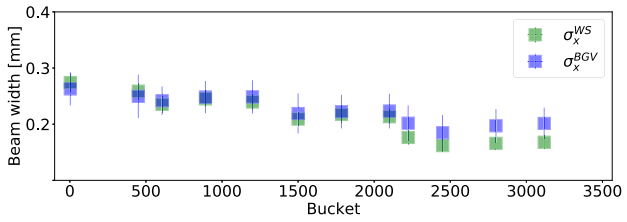

(a) BGV and WS beam size measurements

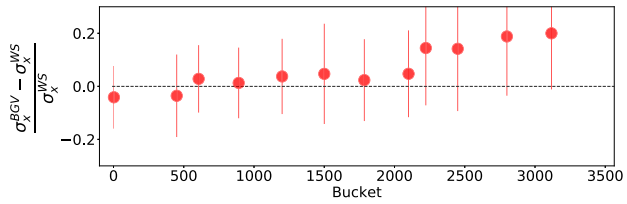

(b) Relative difference between BGV and WS measurements

FIG. 17. BGV and WS beam size measurements comparison for individual LHC proton bunches. Data were taken during a special calibration run at 6.5 TeV.

determined during the acceleration from 0.45 to 6.5 TeV and plotted as a function of time (20 s integration time per data point). Both σ_x^{cor} and σ_y^{cor} are shown in the same figure. For comparison, the solid lines in Fig. 16 show the expected beam size time evolution, assuming no change in the normalized beam emittance. This is given by

$$\sigma(E) = \sigma_{\mathrm{inj}}\sqrt{E_{\mathrm{inj}}/E}, \tag{9}$$

where E_{inj} and σ_{inj} are the energy and beam size, respectively, at injection. The error on the beam size estimation is estimated from the number of events analyzed per data point as explained in the previous section.

D. Measurements per LHC proton bunch

Given the current BGV readout rate, only a few hundred of the 2556 LHC proton bunches can be measured concurrently. While the number of events per bunch for a given integration window is clearly reduced, the expected error in the beam size measurement can still be extrapolated from that presented in the previous section. As an example, Fig. 17 shows measurements during a special calibration run where there were only 12 proton bunches injected in the LHC. The BGV measurements (60 s integration time) are shown together with the corresponding wire scanner (WS); a detailed description of the WS performance can be found in Ref. [39]. The WS measurements are scaled taking into account the accelerator optics functions at the WS and BGV locations.

IX. FUTURE DEVELOPMENTS

The present BGV system has demonstrated its capability to accurately measure beam size at the LHC throughout the acceleration cycle. In order to allow for measurements of smaller beam sizes and/or with greater precision, a series of improvements is foreseen.

Changing the target gas from neon (20.2 atomic mass) to argon (39.9 atomic mass) will increase the trigger rate by approximately 50% with a similar increase in event track multiplicity. The combination of these two factors will considerably reduce the integration time required for precise measurements. In order to be able to provide online beam size measurements with such an increased trigger rate, the BGV system would require a faster data acquisition system and a more powerful HLT computer farm.

The spatial resolution of the reconstructed IP and vertex is directly affected by any multiple scattering of the detected particles between the beam-gas interaction vertex and the detection planes. In the BGV system, the exit window is the main contributor to multiple scattering. A redesign to maintain its thickness to less than 1 mm over its full surface would result in a 30%–50% reduction in multiple scattering effects. A further reduction, by a factor of 2, can be achieved if the aluminum window is replaced by beryllium. New, low-mass, particle detectors could also be considered to further reduce multiple scattering effects in the BGV system.

The addition of a fine timing detector would also allow the BGV system to measure the longitudinal beam size. Given that the LHC bunch length has an rms of 300 ps, a timing resolution of about 50 ps would be sufficient to obtain the longitudinal profile.

X. CONCLUSIONS

An innovative transverse beam size measurement instrument has been presented. Installed in the LHC, both the x and y sizes of the beam can be measured independently, with a precision of better than 2% for an integration time of less than 30 s. The current BGV system can measure sizes varying from about 100 to 1000 μm. This fact, together with the relatively short integration times required, allows beam size monitoring during all operational phases, including the energy ramp. Intensity variations are just reflected in the rate of beam-gas interactions and affect only the integration time needed for a given precision. Higher accelerator energies result in smaller beam sizes that can be easily accommodated by selecting track detectors with an appropriate spatial resolution. The BGV instrument has therefore been demonstrated to provide a novel and effective alternative for beam size monitoring in high-energy colliders, with possible application in a variety of current and future hadron accelerators.

ACKNOWLEDGMENTS

This work has been supported by the HL-LHC project. We thank the LHCb Collaboration, in particular, G. Corti for her support in setting up the BGV simulation package,

F. Alessio for helping with the timing system, and M. Frank, C. Gaspar, L. Granado Cardoso, B. Jost, and N. Neufeld for their support in the development of the BGV data acquisition and experimental control systems.

[1] G. Apollinari *et al.* (HiLumi LHC Collaboration), Technical Report No. CERN-ACC-2014-0300, CERN, 2014.
[2] M. Ferro-Luzzi, Proposal for an absolute luminosity determination in colliding beam experiments using vertex detection of beam–gas interactions, Nucl. Instrum. Methods Phys. Res., Sect. A **553**, 388 (2005).
[3] C. Barschel, Ph.D. thesis, RWTH Aachen University, Germany, 2014, CERN-THESIS-2013-301.
[4] R. Aaij *et al.* (LHCb Collaboration), LHCb detector performance, Int. J. Mod. Phys. A **30**, 1530022 (2015).
[5] D. A. Bartkoski, C. Deibele, and Y. Polsky, Design of an ionization profile monitor for the SNS accumulator ring, Nucl. Instrum. Methods Phys. Res., Sect. A **767**, 379 (2014).
[6] T. Tsang, D. Gassner, and M. Minty, Residual gas fluorescence monitor for relativistic heavy ions at RHIC, Phys. Rev. ST Accel. Beams **16**, 102802 (2013).
[7] V. Tzoganis, H. D. Zhang, A. Jeff, and C. P. Welsch, Design and first operation of a supersonic gas jet based beam profile monitor, Phys. Rev. Accel. Beams **20**, 062801 (2017).
[8] B. Dehning *et al.*, Technical Report No. LHC-BGV-EC-0002 v.1.0, CERN, 2014.
[9] M. Tanabashi *et al.* (Particle Data Group), Review of particle physics, Phys. Rev. D **98**, 030001 (2018).
[10] J. Carvalho, Compilation of cross sections for proton–nucleus interactions at the HERA energy, Nucl. Phys. **A725**, 269 (2003).
[11] O. S. Brüning, P. Collier, P. Lebrun, S. Myers, R. Ostojic, J. Poole, and P. Proudlock, *LHC Design Report*, CERN Yellow Reports: Monographs (CERN, Geneva, 2004).
[12] P. Magagnin, CERN Technical Report No. CERN-EDMS 1568314, 2016.
[13] P. Magagnin and G. Schneider, Technical Report No. CERN-EDMS 1395117, CERN, 2015.
[14] P. Barbosa-Marinho *et al.* (LHCb Collaboration), Technical Report No. CERN-LHCC-2014-001, CERN, 2014.
[15] A. Kuonen, O. Girard, and G. Haefeli, Technical Report No. LPHE-2015-001, EPFL, 2015.
[16] V. Salustino Guimaraes, Ph.D. thesis, Rio de Janeiro Federal University, Brazil, 2012, CERN-THESIS-2012-430.
[17] P. Hopchev *et al.*, Technical Report No. LHC-BGV-EC-0003 v.1.0, CERN, 2015.
[18] P. Hopchev *et al.* (BGV Collaboration), BGV detector installation and alignment, https://twiki.cern.ch/twiki/bin/view/BGV/DetInstallAlign.
[19] P. Barbosa-Marinho *et al.* (LHCb Collaboration), LHCb Technical Design Report No. CERN-LHCC-2001-0011, CERN, 2001.
[20] M. Rihl, Ph.D. thesis, Vienna Technische Universität, 2018, CERN-THESIS-2018-049.
[21] P. Barbosa-Marinho *et al.* (LHCb Collaboration), LHCb Technical Design Report No. CERN-LHCC-2001-040, CERN, 2001.
[22] C. Gaspar *et al.*, Configuring and automating an LHC experiment for faster and better physics output, in *Proceedings of the 16th International Conference on Accelerator and Large Experimental Physics Control Systems (ICALEPCS 2017): Barcelona, Spain, 2017* (JACoW, Geneva Switzerland, 2018), THDPL01, DOI: 10.18429/JACoW-ICALEPCS2017-THDPL01.
[23] S. Lochner and M. Schmelling, Technical Report No. CERN-LHCb-2005-105, CERN, 2006.
[24] G. Haefeli, A. Bay, A. Gong, H. Gong, M. Muecke, N. Neufeld, and O. Schneider, The LHCb DAQ interface board TELL1, Nucl. Instrum. Methods Phys. Res., Sect. A **560**, 494 (2006).
[25] O. Girard, L. An, A. Kuonen, H. Li, and G. Haefeli, Technical Report No. LPHE-2016-02, EPFL, 2016.
[26] O. Girard, Ph.D. thesis, EPFL, 2018, CERN-THESIS-2018-232.
[27] R. Aaij *et al.* (LHCb VELO Group), Performance of the LHCb vertex locator, J. Instrum. **9**, P09007 (2014).
[28] K. Akiba, J. Borel, J. Buytaert, L. Eklund, and M. Gersabeck, Technical Report No. CERN-LHCb-2008-015, CERN, 2007.
[29] S. Giani, G. Haefeli, C. Joram, M. Tobin, and Z. Xu, Technical Report No. CERN-LHCb-PUB-2014-025, CERN, 2014.
[30] G. Haefeli and A. Gong, Technical Report No. CERN-EDMS 690585, EPFL, 2006.
[31] R. Jacobsson, Technical Report No. LHCb-TALK-2002-044, CERN, 2002.
[32] O. Girard, L. An, A. Kuonen, and G. Haefeli, Technical Report No. LPHE-2016-04, EPFL, 2016.
[33] R. Mankel, Technical Report No. CMS-AN-2010/196, DESY, 2010.
[34] S. Donati and L. Ristori, Technical Report No. CDF-Note-4189, FERMILAB, 2003.
[35] M. Clemencic, G. Corti, S. Easo, C. R. Jones, S. Miglioranzi, M. Pappagallo, and P. Robbe (LHCb Collaboration), The LHCb simulation application, Gauss: Design, evolution and experience, J. Phys. Conf. Ser. **331**, 032023 (2011).
[36] M. Gyulassy and X.-N. Wang, HIJING 1.0: A Monte Carlo program for parton and particle production in high energy hadronic and nuclear collisions, Comput. Phys. Commun. **83**, 307 (1994).
[37] G. Trad, Ph.D. thesis, Grenoble University, 2014, CERN-THESIS-2014-390.
[38] R. Alemany-Fernández *et al.*, Cross-Calibration of the LHC Transverse Beam-Profile Monitors, in *Proceedings of the 8th International Particle Accelerator Conference, Copenhagen, Denmark, 2017* (JACoW, Geneva Switzerland, 2017), MOPAB130, DOI: 10.18429/JACoW-IPAC2017-MOPAB130.
[39] F. Roncarolo, Ph.D. thesis, EPFL, 2005, CERN-THESIS-2005-082.